Phase Noise Measurement of RF Signals by Photonic Time Delay and Digital Phase Demodulation

Jingzhan Shi, Fangzheng Zhang, *Member, IEEE*, and Shilong Pan, *Senior Member, IEEE*

***Abstract*— A simple and high-sensitivity frequency–discriminator-based phase noise measurement system using photonic time delay and digital phase demodulation is comprehensively investigated and experimentally demonstrated. By applying a low-loss optical fiber to provide a large amount of time delay, high phase noise measurement sensitivity and large operation bandwidth are guaranteed. Meanwhile, digital phase demodulation is employed to avoid sophisticated feedback control and complex calibration required in conventional frequency-discriminator-based phase noise measurement scheme, which not only eliminates the phase noise measurement error introduced by the feedback loop but also suppresses the influence of the amplitude noise in the signal under test. In addition, a solution for the in-phase and quadrature mismatch problem in the digital phase demodulation is proposed. An experiment is performed. Accurate phase noise measurement is achieved in a large bandwidth from 2 to 35 GHz. With a 2-km single-mode fiber serving as the delay line, phase noise measurement sensitivity as low as −134 dBc/Hz at 10 kHz is achieved at a RF frequency of 10 GHz. The phase noise sensitivity can be further improved by applying a longer fiber. The proposed system is simple, accurate, and stable, and can be applied for analysis of high-frequency and ultralow phase noise microwave signal sources.**

***Index Terms*— Digital phase demodulation, frequency discriminator, microwave photonics, phase noise measurement, photonic delay line.**

I. Introduction

SINGLE-FREQUENCY microwave or millimeter-wave signal source is widely used in modern communications, radars and instrumentation systems. Typically, the performance of a microwave or millimeter-wave system is highly dependent on the quality of RF sources [1], [2]. Phase noise, which denotes the short-term stability of a RF source, is one of the most important specifications to evaluate the quality of the RF source [3]. Simple and high sensitivity phase noise measurement is therefore of great importance for the optimal design of high-performance microwave and millimeter-wave sources. Up to now, there are generally three methods developed to measure the phase noise of a signal source, i.e., direct spectrum method, phase-detector method, and frequency-discriminator method [4], [5]. Direct spectrum method is simple, but it cannot distinguish between phase noise and amplitude noise. Besides, the phase noise measurement sensitivity is usually limited by the spectrum analyzer [4]. In the phase-detector method, a high-quality reference source with phase noise remarkably lower than that of the measured signal is required, making it highly demanding when measuring a signal source with ultralow phase noise [5]. The frequency-discriminator method, in contrast, does not need a reference source. The signal under test (SUT) is first split into two branches, one of which is delayed by a certain time and then mixed with the signal in the other branch [6]. By introducing a large time delay between the two branches, the frequency-discriminator method can achieve much better phase noise measurement sensitivity compared with the previous two methods.

The conventional microwave frequency discriminator is established based on an electrical delay line, which is short (or with large power loss) and narrowband. Optical fiber is an optimal replacement of the electrical delay line because a large time delay can be achieved with very low loss (∼0.2 dB/km) and broad bandwidth (>10 THz). Since the optical fiber delay line was applied for phase noise measurement in a frequency discriminator by E. Rubiola *et al.* [7], considerable efforts have been devoted to improving the performance of the photonics-based phase noise measurement systems [8]–[15]. These improvements are usually implemented by replacing certain electrical components in the frequency discriminator with their photonic counterparts. For instance, in [12], the electrical phase shifter and mixer are replaced by a photonic microwave phase shifter and mixer, respectively. Thanks to the broadband microwave photonic signal processing [16], the operational bandwidth of the phase noise measurement system is dramatically increased.

Despite all these improvements, there are other factors restricting the performance of the frequency-discriminator-based phase noise measurement, especially the use of feedback loops and phase detectors. The feedback loop is established to ensure that the two inputs of the phase discriminator are orthogonal to each other by dynamically controlling an electrical or microwave photonic phase shifter. The use of the feedback loop not only complicates the system configuration,

Manuscript received November 13, 2017; revised March 25, 2018; accepted May 6, 2018. Date of publication May 31, 2018; date of current version September 4, 2018. This work was supported in part by the NSFC Program under Grant 61527820, in part by the Postgraduate Research and Practice Innovation Program of Jiangsu Province under Grant KYCX17_0289, and in part by the Fundamental Research Funds for the Central Universities under Grant NS2018028. *(Corresponding authors: Fangzheng Zhang; Shilong Pan.)*

The authors are with the Key Laboratory of Radar Imaging and Microwave Photonics, Ministry of Education, Nanjing University of Aeronautics and Astronautics, Nanjing 210016, China (e-mail: zhangfangzheng@nuaa.edu.cn; pans@ieee.org).

Color versions of one or more of the figures in this paper are available online at http://ieeexplore.ieee.org.

Digital Object Identifier 10.1109/TMTT.2018.2838119

but also influences the phase noise to be measured, resulting in an inaccurate measurement. The phase detector usually consists of a mixer and a low pass filter (LPF), which converts the phase difference between the two input signals into a voltage that can be measured. However, the conversion factor is related to the power and frequency of the inputs of the mixer, which not only makes the calibration intricate but also introduces amplitude-noise-related measurement errors.

To overcome these problems, phase noise measurement systems using digital phase demodulation were proposed [17]–[20]. By using digital phase demodulation, the phase noise information can be extracted from digital samples of the in-phase and quadrature (I/Q) baseband signals obtained from an I/Q mixer. The major advantage of using digital phase demodulation technology is that the feedback loop and the phase shifter are avoided. However, the time delay is still provided by a short electrical delay line in [17] and [18], which significantly limits the phase noise measurement sensitivity and bandwidth. Besides, the conversion factor of the mixer needs to be calibrated in [18]. In order to measure the conversion factor, two direct-current (dc) blocks are added in [18]. However, the dc block would inevitably affect the close-to-zero-frequency spectrum, which introduces phase noise measurement errors at low offset frequencies. Gheidi and Banai [18] also pointed out that the I/Q mismatch in the digital phase demodulation could lead to measurement errors, but did not provide any solution. In [19], a phase noise measurement system based on photonic-assisted I/Q mixing was reported, which provides a large operation bandwidth and a good sensitivity. However, an additional procedure of replacing a 90° hybrid by a 180° hybrid is required for each measurement to eliminate the dc interferences introduced by the photonic-assisted I/Q mixer, which dramatically complicates the measurement process. Recently, we have proposed a phase noise measurement system based on photonic time delay and digital phase demodulation, which is free of dc interferences [20]. However, only some preliminary experimental observations were reported, and the I/Q mismatch problem in the digital phase demodulation exists. In addition, the photonic time delay is usually sensitive to the environmental change, but the measurement in [20] did not take into account the time delay variation.

In this paper, we perform a comprehensive theoretical and experimental study on the method proposed in [20], with an emphasis on the influence of the I/Q mismatch problem and the time delay variation problem. Solution to the I/Q mismatch problem is proposed by using a variable optical delay line (VODL) and digital compensation, and the time delay variation due to the optical fiber delay line is reduced through a thermostat. This paper is organized as follows. In Section II, a brief introduction of the conventional frequency-discriminator-based phase noise measurement method and its problems originated from the phase detector and the feedback loop is presented. In Section III, the basic principle of the proposed phase noise measurement system is described and the effect of variation of time delay provided by the long fiber is discussed. In Section IV, the I/Q mismatch problem is investigated and a method to solve the I/Q mismatch problem is presented. In Section V, experimental investigation of the proposed system is presented. The measurement accuracy and operation bandwidth are tested by comparing the results with those obtained by a commercial signal analyzer or those provided by the datasheet. The measurement sensitivity is also investigated and compared to the system using an electrical delay line. In Section VI, we conclude this paper.

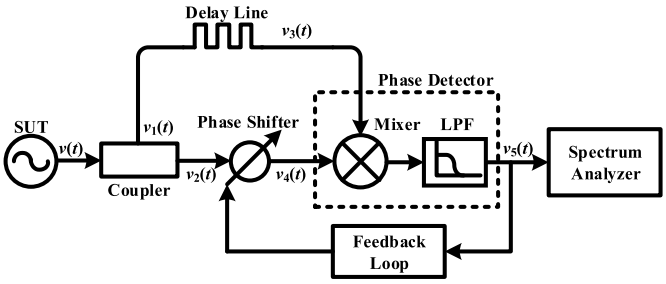

Fig. 1. Schematic of the delay-line-based frequency discriminator system for phase noise measurement. SUT: signal under test. LPF: low pass filter.

II. Typical Frequency Discriminator System

Fig. 1 shows the basic structure of a delay-line-based frequency discriminator system for phase noise measurement. Mathematically, the SUT can be expressed as

$$v(t) = [V_0 + \varepsilon(t)]\cos[2\pi f_0 t + \varphi(t)] \tag{1}$$

where V_0 and f_0 are the amplitude and frequency of the signal, and $\varepsilon(t)$ and $\varphi(t)$ are the amplitude and phase fluctuations, respectively. Through an electrical power divider, the SUT is divided into two equal signals, $v_1(t)$ and $v_2(t)$, respectively, i.e.,

$$v_1(t) = v_2(t) = \frac{\sqrt{2}}{2}[V_0 + \varepsilon(t)]\cos[2\pi f_0 t + \varphi(t)]. \tag{2}$$

In the upper branch, a time delay of τ is introduced by a delay line. The delayed signal is expressed as

$$v_3(t) = \frac{\sqrt{2}}{2}[V_0 + \varepsilon(t-\tau)]\cos[2\pi f_0(t-\tau) + \varphi(t-\tau)] \tag{3}$$

where τ is the time delay.

In the lower branch, a phase shifter controlled by a feedback loop introduces a phase of φ_0 into $v_2(t)$. The introduced phase φ_0 satisfies the condition of "$2\pi f_0\tau + \varphi_0 = 2n\pi + \pi/2$." The phase shifted version of $v_2(t)$ is

$$\begin{aligned} v_4(t) &= \frac{\sqrt{2}}{2}[V_0 + \varepsilon(t)]\cos[2\pi f_0 t + \varphi(t) + \varphi_0] \\ &= -\frac{\sqrt{2}}{2}[V_0 + \varepsilon(t)]\sin[2\pi f_0(t-\tau) + \varphi(t)]. \end{aligned} \tag{4}$$

Then, $v_3(t)$ and $v_4(t)$ are sent to a phase detector that consists of a mixer and a LPF. The voltage at the output of the phase detector is

$$v_5(t) = k_\varphi \sin[\varphi(t) - \varphi(t-\tau)] \approx k_\varphi[\varphi(t) - \varphi(t-\tau)] \tag{5}$$

where k_φ is a constant equal to the slope of the voltage-phase characteristic curve at the zero crossing, and its value is closely related to the power of the SUT [3].

The power spectral density (PSD) of $v_5(t)$ is then given by

$$\begin{aligned} S_v(f_m) &\approx k_\varphi^2[\varphi(t)-\varphi(t-\tau)]_{\text{PSD}} \\ &= k_\varphi^2 \mathbf{E}[|\mathbf{FT}[\varphi(t)-\varphi(t-\tau)]|^2] \\ &= k_\varphi^2 |1-e^{-j2\pi f_m \tau}|^2 \ \mathbf{E}[|\mathbf{FT}[\varphi(t)]|^2] \\ &= k_\varphi^2 |1-e^{-j2\pi f_m \tau}|^2 \ S_\varphi(f_m) \end{aligned} \tag{6}$$

where $\mathbf{FT}[\varphi(t)] = \lim_{T\to\infty} \int_{-T}^{T} \varphi(t) e^{-j2\pi f_m t} dt$ is the Fourier transform of $\varphi(t)$, $\mathbf{E}[\varphi(t)]$ is the expectation value of $\varphi(t)$. Therefore, if the PSD of $v_5(t)$ is measured by a spectrum analyzer, single-sided phase noise spectral density $S_\varphi(f_m)$ is obtained, written as

$$S_\varphi(f_m) = \frac{S_{\text{v}}(f_m)}{k_\varphi^2 |1-e^{-j2\pi f_m \tau}|^2} = \frac{S_{\text{v}}(f_m)}{4k_\varphi^2 \sin^2(\pi f_m \tau)}. \tag{7}$$

Accordingly, the phase noise $L(f_m)$ is

$$L(f_m) = \frac{S_\varphi(f_m)}{2} = \frac{S_v(f_m)}{8k_\varphi^2 \sin^2(\pi f_m \tau)}. \tag{8}$$

According to (8), the phase noise of the SUT can be figured out through dividing the measured $S_v(f_m)$ by a coefficient of 8 $k_\varphi^2 \sin^2(\pi f_m \tau)$. Previously, this coefficient was acquired by a calibration process using a signal source with known phase noise or a determined phase-modulated or frequency-modulated signal source [8]. Theoretically, the amplitude and frequency of the signal source used for calibration should be the same as those of the SUT. As a result, calibration is required for each measurement, which would greatly complicate the phase noise measurement.

Another issue associated with the system in Fig. 1 is the use of feedback loop, which plays an important role to track and correct environment-variation-induced phase drift within the loop bandwidth. However, the phase noise to be measured is essentially a kind of phase drift. Therefore, the use of feedback loop would inevitably suppress the phase noise of the SUT within the bandwidth of the feedback loop, and hence degrade the measurement accuracy. To solve this problem, inverse correction should be applied, which also complicates the measurement.

As described above, the calibration required for each measurement and the feedback loop not only complicate the measurement, but also degrade the measurement accuracy. Therefore, it is highly desired to develop a high-sensitivity phase noise measurement system without any feedback loop and complex calibration in each measurement. In this paper, a method applying photonic time delay and digital phase demodulation is proposed, as demonstrated in the following sections.

III. Principle of the Proposed Method

Fig. 2 shows the schematic of the proposed phase noise measurement system using photonic time delay and digital phase demodulation. Compared with the system in Fig. 1, the proposed system requires a 90° hybrid and two phase

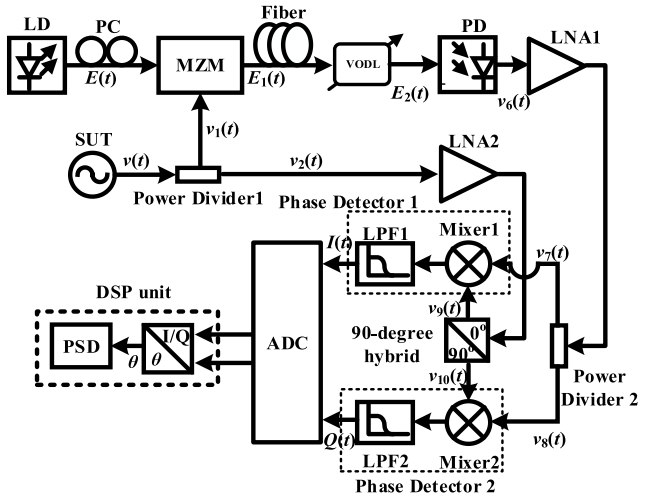

Fig. 2. Schematic of the proposed phase noise measurement system using photonic time delay and digital phase demodulation. LD: laser diode. PC: polarization controller. MZM: Mach–Zehnder modulator. VODL: variable optical delay line. PD: photodetector. LNA: low noise amplifier. ADC: analog-to-digital converter. PSD: power spectral density.

detectors. Besides, a synchronized two-channel analog-to-digital converter (ADC) and a digital signal processing (DSP) unit are needed for data acquisition and processing, respectively. In Fig. 2, the delay line is realized by a length of optical fiber. To do this, the SUT is modulated onto the intensity of an optical carrier from a laser diode (LD) at a Mach–Zehnder modulator (MZM). This optical intensity modulated signal is delayed by a span of fiber and then converted back to the electrical domain at a photodetector (PD). Last, a VODL is added after the fiber to deal with I/Q mismatch problem.

The electrical field of the optical carrier from the LD can be written as

$$E(t) = E_0 \cos(2\pi f_c t) \tag{9}$$

where E_0 is the amplitude and f_c is the frequency. The SUT is also denoted by (1), which is divided by an electrical power divider (Power Divider 1) into two equal signals denoted by (2). In the upper branch, the light source $E(t)$ is intensity-modulated by $v_1(t)$ at the MZM, which is biased at quadrature. The output signal from the MZM is given by

$$\begin{aligned} E_1(t) \approx{}& \sqrt{L_1} E_0 \cos(2\pi f_{\text{c}} t) \\ &\cdot \left\{ \frac{\sqrt{2}}{2} J_0(\alpha) - \sqrt{2} J_1(\alpha) \cos[2\pi f_0 t + \varphi(t)] \right\} \end{aligned} \tag{10}$$

where L_1 is the optical insertion loss of the polarization controller and the MZM. α is the modulation index of the MZM, given by $\alpha = \pi(2M)^{1/2}[V_0 + \varepsilon(t)]/4V_\pi$, where M and V_π are the RF insertion loss and half-wave voltage of the MZM, respectively.

In small signal condition, i.e., $\pi(2M)^{1/2}[V_0 + \varepsilon(t)] << 4V_\pi$ or $\alpha << 1$, the Bessel functions $J_0(\alpha) \approx 1$ and $J_1(\alpha) \approx \alpha/2$. Equation (10) can be rewritten as

$$E_1(t) \approx \frac{\sqrt{2}}{2} \sqrt{L_1} E_0 \cos(2\pi f_c t) \cdot \{1 - \alpha \cos[2\pi f_0 t + \varphi(t)]\}. \tag{11}$$

By introducing a time delay of τ after the fiber, (11) becomes

$$E_2(t) \approx \frac{\sqrt{2}}{2}\sqrt{L_1}\sqrt{L_2}E_0\cos[2\pi f_c(t-\tau)] \cdot\{1-\alpha\cos[2\pi f_0(t-\tau)+\varphi(t-\tau)]\} \quad (12)$$

where L_2 is the insertion loss of the fiber. Then, the signal is detected by a PD with a responsivity of R. The voltage from the PD is written as

$$v_6(t) = Z_L R[E_2(t)\cdot E_2^*(t)] \quad (13)$$

where Z_L is the input impendence. Substituting (12) into (13) and ignoring the dc and $2f_0$ terms, the recovered electrical signal is given by

$$v_6(t) = \frac{-Z_L R L_1 L_2 E_0^2 \alpha}{2}\cdot\cos[2\pi f_0(t-\tau)+\varphi(t-\tau)]. \quad (14)$$

After the PD, a low noise amplifier (LNA1) and another power divider (Power Divider 2) are applied to amplify the signal and divide it into two branches, i.e.,

$$\begin{aligned} v_7(t) &= \frac{-\sqrt{2}Z_L R L_1 L_2 E_0^2 \alpha G_1(P_{v6}, f_0)}{4} \cdot\cos[2\pi f_0(t-\tau)+\varphi(t-\tau)] \\ v_8(t) &= \gamma_1(f_0)\frac{-\sqrt{2}Z_L R L_1 L_2 E_0^2 \alpha G_1(P_{v6}, f_0)}{4} \cdot\cos[2\pi f_0(t-\tau)+\varphi(t-\tau)+\varphi_1(f_0)] \end{aligned} \quad (15)$$

where $G_1(P_{v6}, f_0)$ is the gain of LNA1, which is related to the power of $v_6(t)$, i.e., P_{v6}, and the carrier frequency f_0. $\gamma_1(f_0)$ and $\varphi_1(f_0)$ are the frequency-related amplitude mismatch and phase mismatch between $v_7(t)$ and $v_8(t)$ due to the imbalance of Power Divider 2, respectively.

In the lower branch, signal $v_2(t)$ is amplified by LNA2 and split into two signals by a 90° hybrid. The output signals are

$$\begin{aligned} v_9(t) &= \frac{G_2(P_{v2}, f_0)}{2}[V_0+\varepsilon(t)]\cdot\cos[2\pi f_0 t+\varphi(t)] \\ v_{10}(t) &= \gamma_2(f_0)\frac{G_2(P_{v2}, f_0)}{2}[V_0+\varepsilon(t)] \cdot\sin[2\pi f_0 t+\varphi(t)+\varphi_2(f_0)] \end{aligned} \quad (16)$$

where $G_2(P_{v2}, f_0)$ is the gain of LNA2, which is related to the power of $v_2(t)$, i.e., P_{v2}, and the carrier frequency f_0. $\gamma_2(f_0)$ and $\varphi_2(f_0)$ are the frequency-related amplitude mismatch and phase mismatch between $v_9(t)$ and $v_{10}(t)$ due to the mismatch of the 90° hybrid, respectively.

Then, $v_7(t)$ and $v_9(t)$ are mixed by a mixer (Mixer1) and filtered by an LPF (LPF1). The output signal from LPF1 is

$$I(t) = K_1(P_{v7}, P_{v9}, f_0)\cdot\cos[2\pi f_0\tau+\varphi(t)-\varphi(t-\tau)] \quad (17)$$

where $K_1(P_{v7}, P_{v9}, f_0)$ is the response curve of Mixer 1, which is dependent on the power of $v_7(t)$ and $v_9(t)$, i.e., P_{v7} and P_{v9}, and the carrier frequency f_0.

Similarly, the output signal from LPF2 is given by

$$Q(t) = \gamma_3(f_0)K_2(P_{v8}, P_{v10}, f_0) \cdot\sin\begin{bmatrix} 2\pi f_0\tau+\varphi(t)-\varphi(t-\tau)+ \\ \varphi_2(f_0)-\varphi_1(f_0)+\varphi_3(f_0)\end{bmatrix} \quad (18)$$

where $K_2(P_{v8}, P_{v10}, f_0)$ is the response curve of Mixer 2, which is dependent on the power of $v_8(t)$ and $v_{10}(t)$, i.e., P_{v7} and P_{v9}, and the carrier frequency f_0. $\gamma_3(f_0)$ and $\varphi_3(f_0)$ are the frequency-related amplitude mismatch and phase mismatch between $I(t)$ and $Q(t)$ due to different length of the cables connecting the Power Divider 2 to the mixers, the cables connecting the 90° hybrid to the mixers, the cables connecting the two mixers to the LPFs and the cables connecting the two LPFs to the ADC, and different response curves of the two LPFs.

Then, the obtained analog signals $I(t)$ and $Q(t)$ are digitized by the ADC and processed in the DSP unit. In the DSP unit, a phase term is calculated as

$$\begin{aligned} \theta(t) &= 2\pi f_0\tau+\varphi(t)-\varphi(t-\tau) \\ &= \tan^{-1}\left(\frac{\frac{Q(t)}{k_A I(t)}-\sin d_\varphi}{\cos d_\varphi}\right) \end{aligned} \quad (19)$$

where $k_A = \gamma_3(f_0)\ K_2(P_{v8},\ P_{v10},\ f_0,)/K_1(P_{v7},\ P_{v9},\ f_0)$ denotes the amplitude mismatch between $I(t)$ and $Q(t)$, $d_\varphi = \varphi_1(f_0)-\varphi_2(f_0)+\varphi_3(f_0)$ is the phase mismatch between $I(t)$ and $Q(t)$.

Next, the PSD of $\theta(t)$ is calculated as

$$S_\theta(f_m) = [\varphi(t)-\varphi(t-\tau)]_{\mathrm{PSD}}, \quad \text{for} \quad f_m > 0 \quad (20)$$

where $[\varphi(t)-\varphi(t-\tau)]_{\mathrm{PSD}} = \mathbf{E}[|\mathbf{FT}[\varphi(t)-\varphi(t-\tau)]|^2]$ represents the PSD of $\varphi(t)-\varphi(t-\tau)$.

Based on (20), the phase noise $L(f_m)$ is achieved

$$L(f_m) = H(f_m)S_\theta(f_m) \quad (21)$$

where $H(f_m) = 1/[8\sin^2(\pi f_m\tau)]$, and τ is related to the fiber length given by

$$\tau = \sqrt{\varepsilon_r}\frac{L_d}{c} \quad (22)$$

where ε_r is the relative dielectric constant of the fiber, L_d is the length of the fiber, and c denotes the speed of light in vacuum.

It is worth noting that (20) is established under the hypothesis that the value of τ is constant in the measurement. However, the optical fiber length varies with temperature in practice, which causes the variation of τ [21]. Considering the variation of τ, based on (19), the PSD of $\theta(t)$ becomes

$$S_\theta(f_m) = 2\pi f_0[\tau(t)]_{\mathrm{PSD}} + [\varphi(t)-\varphi(t-\tau)]_{\mathrm{PSD}}. \quad (23)$$

Different from (20), $S_\theta(f_m)$ not only contains the PSD of the phase noise deviation, but also the PSD of the time varying τ, which results in phase noise measurement error in a certain offset frequency range (typically <1 kHz) where τ varies. To eliminate the influence of variation in temperature on the time delay τ, the fiber can be put in a thermostat.

IV. I/Q Mismatch Problem and Its Solution

If the amplitude mismatch and phase mismatch between $I(t)$ and $Q(t)$ are not taken into account, the calculated phase term becomes

$$\theta_m(t) = \tan^{-1}\left(\frac{Q(t)}{I(t)}\right). \quad (24)$$

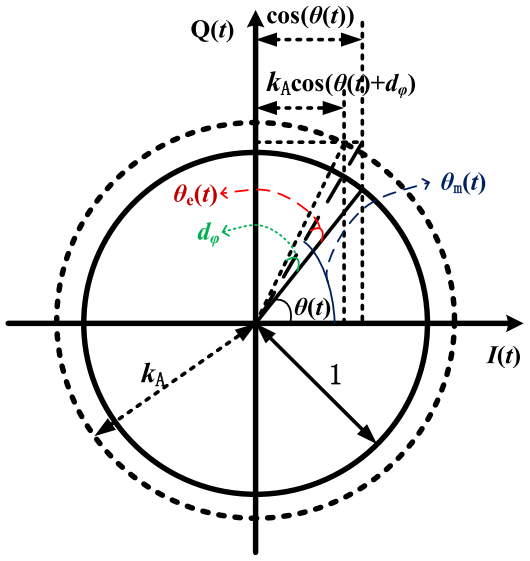

Fig. 3. Calculation of the phase error $\theta_e(t)$ without taking the amplitude mismatch and phase mismatch into consideration.

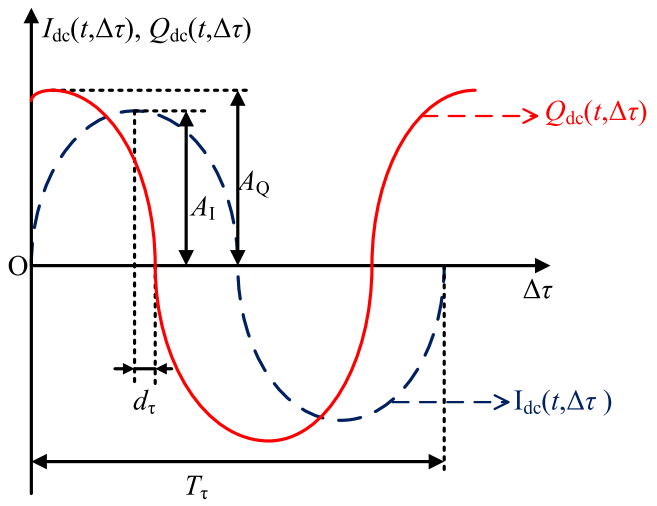

Fig. 4. Schematic of measuring amplitude mismatch and phase mismatch according to the dc values of $I(t, \Delta\tau)$ and $Q(t, \Delta\tau)$.

Fig. 3 shows the phase error $\theta_e(t)$ when the amplitude mismatch and phase mismatch are reckoned without. In the case of small amplitude mismatch and phase mismatch, the phase error can be approximately calculated by

$$\begin{aligned}\theta_e(t) &\approx d_\varphi - \frac{\cos(\theta(t)) - k_A\cos(\theta(t)+d_\varphi)}{k_A} \\ &\approx \theta_{\text{edc}} + k_\theta[\varphi(t) - \varphi(t-\tau)] \end{aligned} \tag{25}$$

where

$$\begin{aligned}\theta_{\text{edc}} &= d_\varphi + \cos(2\pi f_0\tau + d_\varphi) - \frac{1}{k_A}\cos(2\pi f_0\tau) \\ k_\theta &= \left[\frac{1}{k_A}\sin(2\pi f_0\tau) - \sin(2\pi f_0\tau + d_\varphi)\right].\end{aligned}$$

According to (25), the phase term θ_{edc} is not time varying, it has no effect on phase noise measurement for $f_m > 0$. The phase noise measurement error when the amplitude mismatch and phase mismatch are reckoned without is

$$\begin{aligned}L_e(f_m) &= k_\theta^2 H(f_m)[\varphi(t) - \varphi(t-\tau)]_{\text{PSD}} \\ &= k_\theta^2 L(f_m), \quad \text{for} \quad f_m > 0. \end{aligned} \tag{26}$$

So, the phase noise measurement error when amplitude mismatch and phase mismatch are not taken into consideration is not only related to the amplitude mismatch and phase mismatch between $I(t)$ and $Q(t)$, but also related to the carrier frequency f_0, the time delay τ, and the phase noise of SUT $L(f_m)$.

To improve the phase noise measurement accuracy, the phase term $\theta(t)$ ought to be calculated according to (19) by taking the amplitude mismatch and phase mismatch between $I(t)$ and $Q(t)$ into account. The values of k_A and d_φ are different for SUT with different carrier frequencies or powers. So, the mismatches need to be measured for each measurement. The values of k_A and d_φ can be measured without rebuilding the phase noise measurement setup by using the VODL after the fiber in Fig. 2. By changing the length of VODL with a constant speed, an additional small time delay $\Delta\tau$ that changes with time linearly will be introduced. As a result, $I(t)$ and $Q(t)$ can be rewritten as

$$\begin{aligned}I(t, \Delta\tau) &= K_1(P_{v7}, P_{v9}, f_0, T_1) \\ &\quad \cdot\cos[2\pi f_0(\tau + \Delta\tau) + \varphi(t) - \varphi(t-\tau)] \\ Q(t, \Delta\tau) &= \gamma_3(f_0)K_2(P_{v8}, P_{v10}, f_0, T_2) \\ &\quad \cdot\sin\left[\begin{matrix}2\pi f_0(\tau + \Delta\tau) + \varphi(t) - \varphi(t-\tau) \\ +\varphi_2(f_0) - \varphi_1(f_0) + \varphi_3(f_0)\end{matrix}\right]. \end{aligned} \tag{27}$$

Fig. 4 shows the dc values of $I(t, \Delta\tau)$ and $Q(t, \Delta\tau)$ when $\Delta\tau$ changes with time linearly, where $A_I = K_1(P_{v7}, P_{v9}, f_0)$ and $A_Q = \gamma_3(f_0)K_2(P_{v8}, P_{v10}, f_0)$ are the amplitudes of $I(t, \Delta\tau)$ and $Q(t, \Delta\tau)$, respectively, T_τ is the period of $I(t, \Delta\tau)$ or $Q(t, \Delta\tau)$, d_τ is the difference of $\Delta\tau$ when $I(t, \Delta\tau)$ reaches its maximum and when $Q(t, \Delta\tau)$ equals to zero. The values of A_I, A_Q, T_τ, and d_τ are all able to be obtained according to the digitized tracks of $I(t, \Delta\tau)$ and $Q(t, \Delta\tau)$ in the DSP unit. Then, the values of k_A and d_φ can be calculated by

$$\begin{aligned}k_{\text{A}} &= \frac{A_{\text{I}}}{A_{\text{Q}}} \\ d_\varphi &= \frac{d_\tau}{T_\tau}2\pi. \end{aligned} \tag{28}$$

In the proposed system, the calibration process is actually performed by measuring the I/Q mismatch via adjusting the VODL and then compensating the mismatch by (19). The calibration and the measurement can be performed simultaneously. On the one hand, compared to the time delay provided by the long fiber, the time delay introduced by the VODL is negligible. As a result, the value of τ can still be regarded as a constant, indicating that the calibration and the measurement can be realized by the same setup. On the other hand, the change of the phase will be very slow when the VODL is adjusted with a very slow speed, so the frequency of the phase jitter introduced by it can be very small. As a result, the VODL only affects the phase noise measurement result

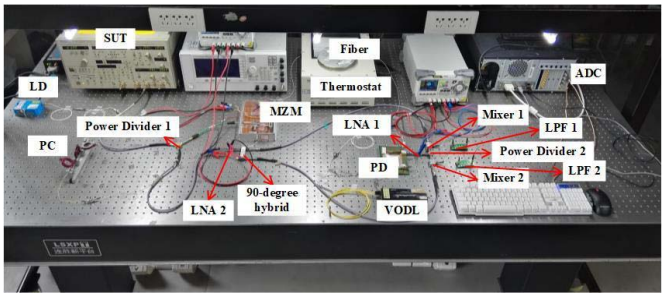

Fig. 5. Photograph of the proposed phase noise measurement system.

at a very low offset frequency (typically less than 10 Hz), which is much lower than the cutoff frequency (typically ~1 kHz) of the feedback loop used in the conventional frequency discriminators.

V. Experiments and Analyses

A. Experimental Setup

To evaluate the performance of the proposed system, an experiment is carried out based on the setup in Fig. 2. The LD (TeraXion Inc.) operates at a wavelength of 1550 nm. A 50-GHz MZM (FUJITSU FTM7938EZ) is applied to perform optical intensity modulation. A 2-km single-mode fiber (SMF) is used to provide the time delay. After the SMF, a VODL (General Photonics Inc., VDL-001-15-600-SM-FC/APC) is applied to measure amplitude mismatch and phase mismatch, which can provide a delay range from 0 to 600 ps. A PD (FINISAR U^2T) with a bandwidth of 59 GHz and a responsivity of 0.6 A/W is used to perform optical-to-electrical conversion. The operation bandwidth of the power dividers (Power Divider 1 and Power Divider 2, KRYTAR 6100400) are both from 1 to 40 GHz. The two LNAs (LNA1 and LNA2, B&Z Technologies) can operate over a frequency range from 0.1 to 40 GHz with a gain of 30 dB. The operation frequency of the 90° hybrid (KRYTAR 3017360K) is from 1.7 to 36 GHz. Its amplitude and phase response is measured by a VNA, which shows that the amplitude imbalance was less than 1.7 dB and the phase mismatch was less than 12° over the full frequency range. The two mixers (Mixer1 and Mixer2, Marki M4-0140) and two LPFs (LPF1 and LPF2) are selected with the same parameters, respectively. The RF/LO frequency range of the mixers are both from 1 to 40 GHz. The passband of the LPFs is from 0 to 1 MHz. A four-channel 24-bit ADC (National Instruments PXI-4462) is used to sample and record the data. The sampling rate was set to 204.8 kHz, which means the phase noise measurement offset frequency is below 102.4 kHz. According to the noise analysis in [17], the 24-bit high accuracy ADC helps to maintain a low phase noise floor in a large range of input power level. A photograph of the implemented setup is shown in Fig. 5.

B. Phase Noise Measurement Sensitivity

The phase noise measurement sensitivity is characterized by the phase noise floor. The method for measuring the phase noise floor is as follows. The optical fiber is replaced by an optical attenuator having the same attenuation as the fiber induced power loss. The inherent phase noise of the system is calculated according to (21), which is regarded as the phase noise floor [18].

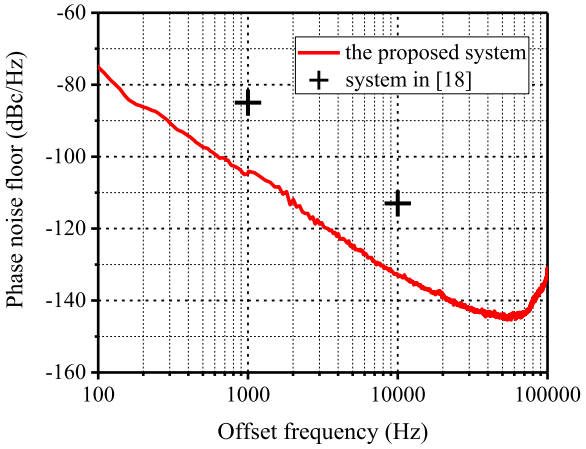

Fig. 6. Phase noise floor of the proposed system using a 2-km SMF (red solid curve) and that of the system in [18] (black marker).

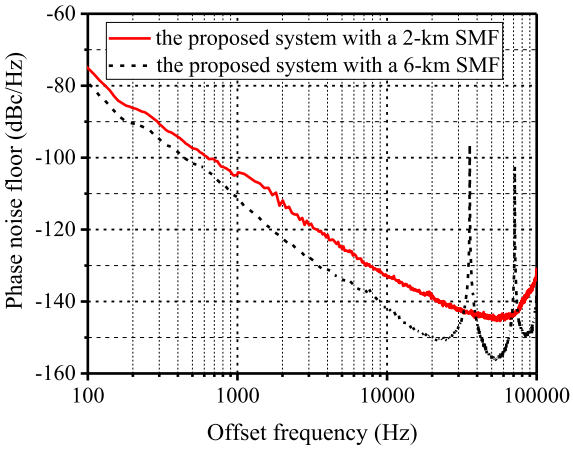

Fig. 7. Phase noise floor of the proposed system and its improved method.

The phase noise floor of the proposed system is measured and shown in Fig. 6. As can be seen, the phase noise floor at 10-GHz RF frequency is −105 dBc/Hz at 1 kHz and −134 dBc/Hz at 10 kHz, respectively. This phase noise measurement sensitivity is greatly improved compared with the system using an electrical delay line [18], where the phase noise floor at 4.9 GHz is −85 dBc/Hz at 1 kHz and −113 dBc/Hz at 10 kHz, respectively, as indicated in Fig. 6.

To further improve the phase noise measurement sensitivity, one method is to increase the time delay τ by applying a longer fiber [8]. When a 6-km SMF is applied in the system, the measured phase noise floor is shown in Fig. 7. Compared with the system using a 2-km SMF, the measurement sensitivity when using a 6-km SMF is improved to be −111 dBc/Hz at 1 kHz and −141 dBc/Hz at 10 kHz, respectively.

C. Verification of Measurement Accuracy

To check the measurement accuracy of the proposed system, the phase noise of a 10-GHz signal generated by Anritsu MP1763C is tested.

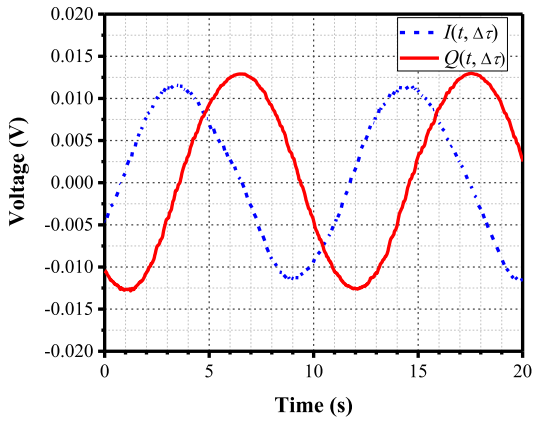

Fig. 8. Measurement of amplitude mismatch k_A and phase mismatch d_φ between I/Q channels before measuring the phase noise of a 10-GHz clock signal.

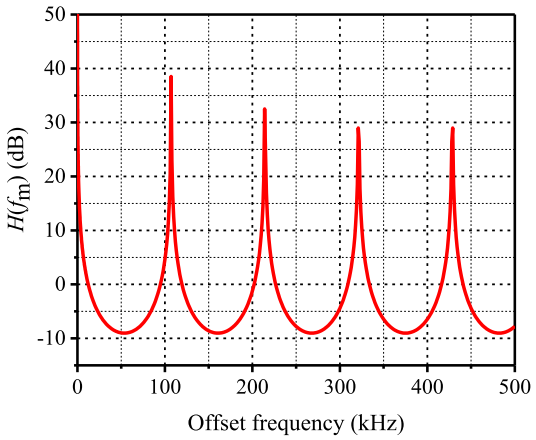

Fig. 10. Calculated $H(f_m)$ in unit of dB.

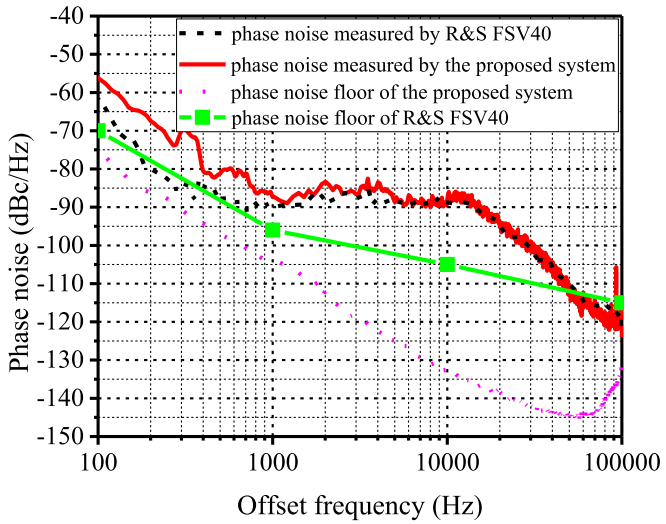

Fig. 9. Phase noise of the 10-GHz clock signal measured by the proposed system (red solid curve) and that measured by a commercial signal analyzer R&S FSV40 (black dashed curve), and phase noise floor of the proposed system (magenta dotted curve) and R&S FSV40 (green solid curve).

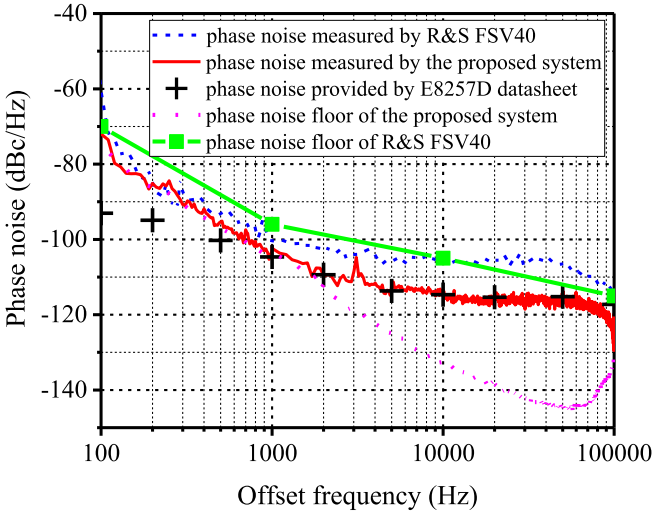

Fig. 11. Phase noise of E8257D according to its datasheet (black marker), measured by the proposed system (red solid curve), and measured by a commercial signal analyzer R&S FSV40 (blue dashed curve), and phase noise floor of the proposed system (magenta dotted curve) and R&S FSV40 (green solid curve).

The amplitude mismatch k_A and phase mismatch d_φ between I/Q channels are measured by changing the length of VODL with a constant speed. The digitalized tracks of $I(t, \Delta\tau)$ and $Q(t, \Delta\tau)$ are shown in Fig. 8. According to (28), the values of amplitude mismatch k_A and phase mismatch d_φ can be calculated as: $k_\mathrm{A} = 1.11$, $d_\varphi = -7.45°$.

The phase noise measurement results are shown in Fig. 9. The result measured by a commercial signal analyzer (R&S FSV40) is also plotted in Fig. 9 as a comparison. In addition, the phase noise floor of the proposed system and R&S FSV40 [22] are also included in Fig. 9. It can be seen that there is a good agreement between the two measurement results, especially for offset frequencies from 1 to 100 kHz.

For offset frequencies between 0.1 and 1 kHz, there is slight deviation between the two curves. This is mainly resulted from the factor $H(f_m) = 1/[8\sin^2(\pi f_m \tau)]$, which has an infinite value at offset frequencies of f_{mN} given by

$$f_{mN}\tau = N, \quad N = 0, 1, 2, \ldots. \tag{29}$$

To clearly explain this effect, Fig. 10 shows the calculated response of $H(f_m)$ of the proposed system. At zero offset frequency, there is an infinite response that causes the deviation at low offset frequencies in Fig. 9. This is a common problem suffered by all frequency-discriminator-based systems.

To further verify the measurement accuracy as well as the good sensitivity of the proposed system, the phase noise of a 10-GHz signal generated from a commercial microwave analog signal generator (Keysight E8257D) is measured, as shown in Fig. 11, where the phase noise measured by a commercial signal analyzer (R&S FSV40) is also included. Besides, the phase noise at specific offset frequencies obtained from the datasheet of the signal generator [23] is indicated in Fig. 11. The phase noise curves in [23] are measured by Keysight E5500 Series, which use phase-detector method for phase noise measurement [24]. The phase noise floor of the proposed system and R&S FSV40 are also shown in Fig. 11. In this situation, precise phase noise measurement is achieved by the proposed system. In contrast, inaccurate measurement

TABLE I
PERFORMANCE COMPARISON BETWEEN THE PROPOSED PHASE NOISE MEASUREMENT SYSTEM AND THE PREVIOUSLY REPORTED SYSTEMS

	Noise Floor @10 kHz (dBc/Hz)	Operation Bandwidth (GHz)	Complexity	I/Q Mismatch Problem
This work	-134	2-35	Low	Solved
[20]	-134	2-35	Low	Not solved
[19]	-131	5-35	High	Not solved
[18]	-113	N/A	High	Not solved
[17]	N/A	W-band	Low	Not solved
[14]	-66 @1 kHz	0.5-9	High	N/A
[12]	-140	5-40	High	N/A
[11]	-137	5-40	High	N/A
[10]	-130	5-40	High	N/A
[9]	-132	N/A	High	N/A

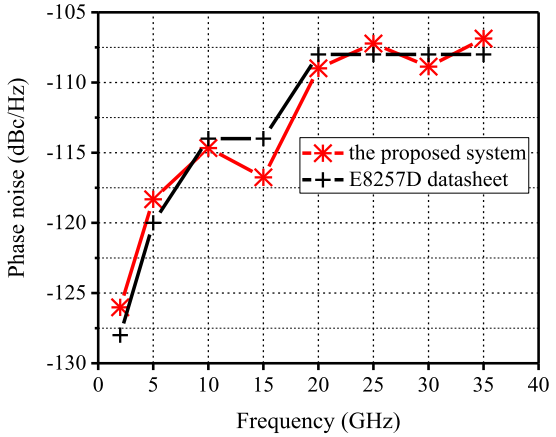

Fig. 12. Phase noises at offset frequency of 10 kHz of a wideband signal source (Keysight E8257D) measured by the proposed system (red marker) and provided by the datasheet (black marker).

by the commercial signal analyzer arises because the signal source has phase noise lower than the measurement sensitivity of the signal analyzer.

D. Operation Bandwidth

In addition to the higher sensitivity, another advantage of the proposed system is the large operation bandwidth. To verify this property, the phase noise of single-frequency signals of some specific frequencies generated by Keysight E8257D is tested.

Fig. 12 shows the measured phase noise at 10-kHz offset frequency when the frequency of SUT changes from 2 to 35 GHz. As a comparison, the values of phase noise provided by the datasheet of E8257D [23] are also plotted in Fig. 12. It can be seen clearly that the differences between the measured results and the values provided by [23] are less than 3 dB. This not only confirms the accuracy of the proposed system again, but also proves that the proposed system can operate at a frequency range from 2 to 35 GHz, which is ultimately determined by the 90° hybrid.

However, even though photonic time delay has been used in the proposed system to replace the electrical delay line, the operation bandwidth is still limited by other electrical components, including the power dividers, the 90° hybrid, the LNAs and the mixers. Zhang *et al.* [19] use a photonic-assisted I/Q mixer to avoid the bandwidth limitation from the electrical mixers. However, the lower limit of the measurement frequency range is determined by the edge slope of the tunable optical bandpass filter used in [19]. As a result, the system in [19] is unavailable to measure sources with carrier frequency less than 5 GHz. In addition, the phenomenon of fiber dispersion-induced RF fading is also a factor limiting the operation bandwidth [25], [26]. According to [26], the fiber dispersion-induced RF fading can be overcome by using a dual-electrode MZM to generate an optical carrier with single sideband modulation.

E. Performance Comparison

Table I lists the performance comparison between the proposed phase noise measurement system and the previously reported systems. Compared with the previously reported systems, the proposed system has several advantages. First, systems in [9]–[12] and [14] suffer from high complexity due to the use of feedback loops and phase detectors, while the proposed system is significantly simplified thanks to the use of digital phase demodulation. Second, compared with the systems in [17]–[20], which also apply digital phase demodulation, the proposed system solves the I/Q mismatch problem. Third, the systems in [9]–[12], [14], and [18] need calibration before each measurement for different SUTs, while the calibration process in the proposed system used to solve the I/Q mismatch problem can be performed simultaneously with the phase noise measurement process, which helps to reduce the complexity of measurement. Finally, different from the systems in [17] and [18], where electrical cables are used as the delay line, the proposed system uses broadband and low-loss optical fiber to provide a large amount of time delay, which helps to achieve a high measurement sensitivity and a broad bandwidth.

VI. CONCLUSION

We have comprehensively investigated and experimentally demonstrated a phase noise measurement method using photonic time delay and digital phase demodulation. The system adopts a low-loss optical fiber to provide a large amount of

time delay and a 90° hybrid to realize digital phase demodulation. Compared to the conventional frequency-discriminator-based phase noise measurement system, the system is free from complex calibration, phase shifter, and feedback loop for phase control, which simplifies both the system configuration and operation complexity. More important, the I/Q mismatch problem in digital phase demodulation technology is investigated and solved. Thanks to the use of optical fiber delay line, a good phase noise measurement sensitivity and a large operation bandwidth are achieved. The phase noise floor is as low as −105 dBc/Hz at 1 kHz and −134 dBc/Hz at 10 kHz at a RF frequency of 10 GHz, which can be further improved by applying a longer fiber. A large operation bandwidth in the range from 2 to 35 GHz is also realized.

The performance of the proposed system in terms of offset frequency range, sensitivity, and operation bandwidth can be further improved. In the proposed system, the offset frequency range is mainly determined by the sampling rate of the ADC, so it can be broadened by adopting an ADC with higher sampling rate. The sensitivity of the proposed system can be further increased by a longer fiber. However, when the fiber length is increased, the reliable offset frequency range for phase noise measurement will be reduced because the frequency spacing between the adjacent infinite points of $H(f_m)$ is also reduced. This problem can be solved by applying a longer fiber for a close to carrier measurement and a shorter fiber for a far from carrier measurement [9]. Another approach to improve the phase noise measurement sensitivity is to apply two-channel cross correlation [13]. The operation bandwidth of the proposed system is eventually determined by the electrical 90° hybrid. An effective way to break this limitation is to employ photonic-assisted I/Q mixers, which are able to realize I/Q mixing without electrical 90° hybrid [27], [28].

REFERENCES

[1] A. G. Armada and M. Calvo, "Phase noise and sub-carrier spacing effects on the performance of an OFDM communication system," *IEEE Commun. Lett.*, vol. 2, no. 1, pp. 11–13, Jan. 1998.

[2] D. B. Leeson and G. F. Johnson, "Short-term stability for a Doppler radar: Requirements, measurements, and techniques," *Proc. IEEE*, vol. 54, no. 2, pp. 244–248, Feb. 1966.

[3] M. Jankovic, "Phase noise in microwave oscillators and amplifiers," Ph.D. dissertation, Dept. Elect., Comput. Energy Eng, Faculty Graduate School, Univ. Colorado, Boulder, CO, USA, 2010.

[4] U. L. Rohde, A. K. Poddar, and A. M. Apte, "Getting its measure: Oscillator phase noise measurement techniques and limitations," *IEEE Microw. Mag.*, vol. 14, no. 6, pp. 73–86, Sep./Oct. 2013.

[5] A. K. Poddar, U. L. Rohde, and A. M. Apte, "How low can they go?: Oscillator phase noise model, theoretical, experimental validation, and phase noise measurements," *IEEE Microw. Mag.*, vol. 14, no. 6, pp. 50–72, Sep./Oct. 2013.

[6] C. Schiebold, "Theory and design of the delay line discriminator for phase noise measurements," *Microw. J.*, vol. 26, no. 12, pp. 103–112, Dec. 1983.

[7] E. Rubiola, E. Salik, S. Huang, N. Yu, and L. Maleki, "Photonic-delay technique for phase-noise measurement of microwave oscillators," *J. Opt. Soc. Amer. B, Opt. Phys.*, vol. 22, no. 5, pp. 987–997, May 2005.

[8] K. Volyanskiy *et al.*, "Applications of the optical fiber to the generation and measurement of low-phase-noise microwave signals," *J. Opt. Soc. Amer. B, Opt. Phys.*, vol. 25, no. 12, pp. 2140–2150, Dec. 2008.

[9] B. Onillon, S. Constant, and O. Liopis, "Optical links for ultra low phase noise microwave oscillators measurement," in *Proc. IEEE Freq. Control Symp.*, Aug. 2005, pp. 545–550.

[10] D. Zhu, F. Zhang, P. Zhou, D. Zhu, and S. Pan, "Wideband phase noise measurement using a multifunctional microwave photonic processor," *IEEE Photon. Technol. Lett.*, vol. 26, no. 24, pp. 2434–2437, Dec. 15, 2014.

[11] D. Zhu, F. Zhang, P. Zhou, and S. Pan, "Phase noise measurement of wideband microwave sources based on a microwave photonic frequency down-converter," *Opt. Lett.*, vol. 40, no. 7, pp. 1326–1329, Apr. 2015.

[12] F. Zhang, D. Zhu, and S. Pan, "Photonic-assisted wideband phase noise measurement of microwave signal sources," *Electron. Lett.*, vol. 51, no. 16, pp. 1272–1274, Aug. 2015.

[13] P. Salzenstein *et al.*, "Realization of a phase noise measurement bench using cross correlation and double optical delay line," *Acta Phys. Polonica A*, vol. 112, no. 5, pp. 1107–1111, Sep. 2007.

[14] W. Wang, J. G. Liu, H. Mei, W. Sun, and N. Zhu, "Photonic-assisted wideband phase noise analyzer based on optoelectronic hybrid units," *J. Lightw. Technol.*, vol. 34, no. 14, pp. 3425–3431, Jul. 15, 2016.

[15] S. Pan and J. Yao, "Photonics-based broadband microwave measurement," *J. Lightw. Technol.*, vol. 35, no. 16, pp. 3498–3513, Aug. 15, 2016.

[16] J. Yao, "Microwave photonics," *J. Lightw. Technol.*, vol. 27, no. 3, pp. 314–335, Feb. 1, 2009.

[17] S. O. Tatu, E. Moldovan, S. Affes, B. Boukari, K. Wu, and R. G. Bosisio, "Six-port interferometric technique for accurate *W*-band phase-noise measurements," *IEEE Trans. Microw. Theory Techn.*, vol. 56, no. 6, pp. 1372–1379, Jun. 2008.

[18] H. Gheidi and A. Banai, "Phase-noise measurement of microwave oscillators using phase-shifterless delay-line discriminator," *IEEE Trans. Microw. Theory Techn.*, vol. 58, no. 2, pp. 468–477, Feb. 2010.

[19] F. Zhang, J. Shi, and S. Pan, "Wideband microwave phase noise measurement based on photonic-assisted I/Q mixing and digital phase demodulation," *Opt. Express*, vol. 25, no. 19, pp. 22760–22768, Sep. 2017.

[20] J. Shi, F. Zhang, and S. Pan, "High-sensitivity phase noise measurement of RF sources by photonic-delay line and digital phase demodulation," presented at the Int. Conf. Opt. Commun. Netw. (ICOCN), Wuzhen, China, Aug. 2017.

[21] N. Shibata, Y. Katsuyama, Y. Mitsunaga, M. Tateda, and S. Seikai, "Thermal characteristics of optical pulse transit time delay and fiber strain in a single-mode optical fiber cable," *Appl. Opt.*, vol. 22, no. 7, pp. 979–984, Apr. 1983.

[22] *R&S FSV-K40 Phase Noise Measurement Application (Data Sheet) Version 02.00*, Rohde Schwarz, Munich, Germany, 2014, p. 4.

[23] *E8257D PSG Microwave Analog Signal Generator Data Sheet*, Keysight Technol., Santa Rosa, CA, USA, 2016, p. 20.

[24] *E5500 Series Phase Noise Measurement Solutions 50 kHz up to 110 GHz Configuration Guide*, Keysight Technol., Santa Rosa, CA, USA, 2016.

[25] H. Schmuck, "Comparison of optical millimeter-wave system concepts with regard to chromatic dispersion," *Electron. Lett.*, vol. 31, no. 21, pp. 1848–1849, Oct. 1995.

[26] G. H. Smith, D. Novak, and Z. Ahmed, "Overcoming chromatic-dispersion effects in fiber-wireless systems incorporating external modulators," *IEEE Trans. Microw. Theory Techn.*, vol. 45, no. 8, pp. 1410–1415, Aug. 1997.

[27] Z. Tang and S. Pan, "Image-reject mixer with large suppression of mixing spurs based on a photonic microwave phase shifter," *J. Lightw. Technol.*, vol. 34, no. 20, pp. 4729–4735, Oct. 15, 2016.

[28] Y. Gao, A. Wen, Z. Tu, W. Zhang, and L. Lin, "Simultaneously photonic frequency downconversion, multichannel phase shifting, and IQ demodulation for wideband microwave signals," *Opt. Lett.*, vol. 41, no. 19, pp. 4484–4487, Oct. 2016.

Jingzhan Shi received the B.S. and M.S. degrees in electrical engineering from the Nanjing University of Aeronautics and Astronautics, Nanjing, China, in 2013 and 2016, respectively. He is currently pursuing the Ph.D. degree at the Key Laboratory of Radar Imaging and Microwave Photonics (Nanjing Univ. Aeronaut. Astronaut.), Ministry of Education, Nanjing.

His current research interests include phase noise measurement of microwave signals.

Fangzheng Zhang (S'10–M'13) received the B.S. degree from the Huazhong University of Science and Technology, Wuhan, China, in 2008, and the Ph.D. degree from the Beijing University of Posts and Telecommunications, Beijing, China, in 2013.

He is currently an Associate Professor with the College of Electronic and Information Engineering, Nanjing University of Aeronautics and Astronautics. His current research interests include microwave photonics, coherent optical communications, and all-optical signal processing.

Shilong Pan (S'06–M'09–SM'13) received the B.S. and Ph.D. degrees in electronics engineering from Tsinghua University, Beijing, China, in 2004 and 2008, respectively.

From 2008 to 2010, he was a "Vision 2010" Post-Doctoral Research Fellow with the Microwave Photonics Research Laboratory, University of Ottawa, Ottawa, ON, Canada. In 2010, he joined the College of Electronic and Information Engineering, Nanjing University of Aeronautics and Astronautics, Nanjing, China, where he is currently a Full Professor and an Executive Director with the Key Laboratory of Radar Imaging and Microwave Photonics, the Ministry of Education. He has authored or co-authored over 340 research papers, including over 180 papers in peer-reviewed journals and 160 papers in conference proceedings. His current research interests include microwave photonics, optical generation and processing of microwave signals, analog photonic links, photonic microwave measurement, and integrated microwave photonics.

Dr. Pan was a recipient of an OSA Outstanding Reviewer Award in 2015. He was a Top Reviewer of the *Journal of Lightwave Technology* in 2016. He is currently a Topical Editor of the *Chinese Optics Letters*. He is a Chair of numerous international conferences and workshops, including the TPC Chair of the International Conference on Optical Communications and Networks in 2015, the TPC Co-Chair of the IEEE International Topical Meeting on Microwave Photonics in 2017, the TPC Chair of the High-Speed and Broadband Wireless Technologies Subcommittee of the IEEE Radio Wireless Symposium in 2013, 2014, and 2016, the TPC Chair of the Optical Fiber Sensors and Microwave Photonics Subcommittee of the OptoElectronics and Communication Conference in 2015, and a Chair of the Microwave Photonics for Broadband Measurement Workshop of the IEEE MTT-S International Microwave Symposium in 2015.